Journal of Materials Chemistry C

ROYAL SOCIETY OF CHEMISTRY

PAPER

View Article Online
View Journal | View Issue

Cite this: J. Mater. Chem. C, 2021, 9, 16290

Supramolecular organic–inorganic domains integrating fullerene-based acceptors with polyoxometalate-bis-pyrene tweezers for organic photovoltaic applications†

Gabriele Giancane, [ab] Simona Bettini, [bc] Ludovico Valli, *[bc] Victoria Bracamonte, [de] Mauro Carraro, [f] Marcella Bonchio *[f] and Maurizio Prato *[ghi]

A strategy to improve organic photovoltaics, and to enhance the device efficiency, builds on the design of interfacial layered (IFL) materials implementing the performance of the photoactive acceptor/donor system. A novel IFL blend has been engineered by a supramolecular organic–inorganic heterojunction integrating polyoxometalate-bis-pyrene (**pyrPOM**) receptors that can selectively bind fullerene-based acceptors through π–π interactions and in particular the most used phenyl-C61-butyric acid methyl ester (**PCBM**) **PCBM**. The resulting **pyrPOM@PCBM** IFL, assembled by means of the Langmuir–Blodgett approach, has been fully characterized both in solution and on solid supports by means of the Langmuir–Schaefer method, featuring a high dielectric function, good polarizability and piezo-responsive behavior, which suggest ferroelectric properties. An organic solar cell is realized interposing the IFL between poly(3-hexylthiophene) (P3HT) as polymer donor and the **PCBM** acceptor layers, thus enhancing the open circuit voltage of the solar device by about 34% under an applied bias of ±5 V.

Received 6th July 2021,
Accepted 9th August 2021

DOI: 10.1039/d1tc03148a

rsc.li/materials-c

Introduction

The pioneering work of Hummelen and Wudl in the field of fullerene materials has produced the first, most used, and still unmatched molecular acceptor for applications in organic photovoltaics (OPV), a key technology for the next generation transition toward renewable solar energy conversion.[1]

Indeed, the fullerene derivative phenyl-C61-butyric acid methyl ester (**PCBM**) has been extensively used in combination with poly(3-hexylthiophene) (P3HT) as polymer donor for the fabrication of P3HT:**PCBM** photoactive blends or thin layers with nanostructured and interpenetrating morphologies. Molecular control on the acceptor–donor (A:D) components and their processing play a fundamental role for the OPV performance, having a direct impact on light absorption, exciton dissociation, charge transport, and charge recombination events.[2]

While highly attractive for the low cost-fabrication, scalability, light weight and flexibility, OPV suffers one major intrinsic limitation with respect to inorganic solar cells. This is due to the low dielectric constant (ε_r) of organic semiconductor and photoactive blends, with values ($\varepsilon_r \approx 3$) remarkably lower than inorganic materials ($\varepsilon_r > 10$). This feature prevents an efficient separation of photogenerated excitons, strongly bound by their mutual coulombic attraction.[3–8]

To improve the OPV performance, and mitigate the organic materials downsides, a viable strategy is offered by the engineering of interfacial layer (IFL) materials. IFL can open new routes for shaping both the morphology and contacts of the photoactive A:D systems. At the same time it tunes the band alignment, enhances the built-in electric field in order to counteract charge recombination, minimizes interfacial losses and improves stability.[9,10]

[a] Department of Cultural Heritage, University of Salento, Via D. Birago, 73100, Lecce, Italy
[b] Consorzio Interuniversitario Nazionale per la Scienza e Tecnologia dei Materiali, INSTM, Via G. Giusti, 9, I-50121 Firenze, Italy. E-mail: ludovico.valli@unisalento.it
[c] Department of Biological and Environmental Sciences and Technologies, DISTEBA, University of Salento, Via per Arnesano, 73100 Lecce, Italy
[d] Universidad Nacional de Córdoba. Facultad de Matemática, Astronomía, Física y Computación, Córdoba, Argentina
[e] CONICET, Instituto de Física Enrique Gaviola (IFEG), Córdoba, Argentina
[f] CNR-ITM and Dipartimento di Scienze Chimiche, University of Padova, Padova, Italy. E-mail: marcella.bonchio@unipd.it
[g] Department of Chemical and Pharmaceutical Sciences, CENMAT, Center of Excellence for Nanostructured Materials, INSTM UdR Trieste, Trieste, University of Trieste, via Licio Giorgieri 1, 34127 Trieste, Italy. E-mail: prato@units.it
[h] Center for Cooperative Research in Biomaterials (CIC biomaGUNE) Basque Research and Technology Alliance (BRTA), Paseo de Miramón 194, Donostia San Sebastián E-20014, Spain
[i] Basque Foundation for Science, Ikerbasque, Bilbao E-48013, Spain

† Electronic supplementary information (ESI) available. See DOI: 10.1039/d1tc03148a

IFL based on inorganic polyoxometalates (POMs) have been successfully applied as electron injection/extraction interlayers in photo-electro devices including organic photovoltaic cells. POMs are highly charged, polyanionic, molecular metal oxides characterized by nano-sized dimensions and a rich supramolecular and covalent surface chemistry.[11,12] Their tunable structural properties, unique multi-electron acceptor properties, charge mobility, processability and robustness offer a valuable opportunity for the fabrication of IFLs wherein POMs are sandwiched between the electrodic semiconductor surface and the photoactive organic layers, leading to enhanced performances.[13–19]

In particular, electron-rich lacunary POMs (mono-vacant α-$PM_{11}O_{39}^{7-}$ with M = W or Mo and tri-vacant α-$PW_9O_{34}^{9-}$ structures) have been used to grow multifunctional IFLs (10 nm thickness) between the electron acceptor layers (cathode, TiO_2) and the organic photoactive film containing poly(3-hexylthiophene donors (P3HT or PTB7) and fullerene-based acceptors ($PC_{70}BM$ or an indene-C_{60} bis-adduct, $IC_{60}BA$), resulting in the performance enhancement of a polymer solar cell. A remarkable power conversion efficiency (PCE) increase, up to 33%, was obtained with respect to the POM-free set-up. In this asset, the POM-based IFL provides a multi-functional leverage for (i) reducing the TiO_2 work function (W_F), (ii) inducing electron mobility, (iii) improving morphology and physical contact, (iv) reducing interfacial recombination losses and (v) favoring an effective exciton dissociation at the photoactive blend interfaces.[20]

As far as the direct modification of the A:D heterojunction components is concerned, recent studies have explored the evolution to multi-phase domains. This has allowed researchers to go beyond the classical two-phase mixture in order to improve charge separation and transport, generally requiring a cascade order and connectivity of donor–acceptor sites. With this aim, the blend morphology has been tuned to include pure donor and acceptor domains bridged by mixed regions.[21–26] Moreover, multi-acceptor/donor heterojunctions have offered a way to overcome binary A:D components thus improving the OPV performance.[27]

Building on these concepts, we propose herein a novel approach for OPV enhancement, based on the supramolecular engineering of an organic–inorganic IFL integrating POM installed bis-pyrene tweezer receptors that can selectively bind the **PCBM** core.[28]

Our results address the host–guest interactions between the bis-pyrene-tagged decatungstosilicate $^n(Bu_4N)_4[\{(C_{16}H_9)SO_2NH(CH_2)_3Si\}_2O(\gamma\text{-}SiW_{10}O_{36})]$ (hereafter named **pyrPOM**) and **PCBM** (Fig. 1 and Fig. S1, ESI†), their binding stoichiometry and the multi-redox behavior of the molecular assembly. The resulting supramolecular film behaves as a tunable dipole layer, exhibiting ferroelectric polarization properties to induce a strong electric field into the A:D photoactive layers and tune their energy levels for increasing the OPV efficiency.[29]

The co-localization of the inorganic POM scaffold with the fullerene cores, regulated by the bis-pyrene tweezer receptor is expected to direct the IFL molecular architecture and morphology, while imparting a favorable polarization of the charge density between the organic–inorganic domains. The ordering of **pyrPOM:PCBM** architecture lies at the origin of the ferroelectric behavior, as it turns out that the polarization direction can be switched between two opposite states upon application of a voltage pulse.[28]

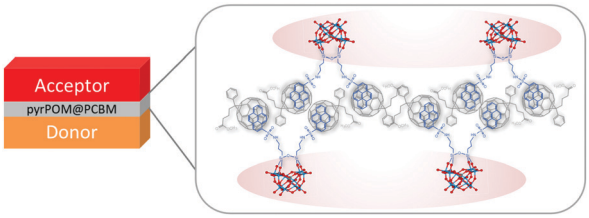

Fig. 1 Stacking layers configuration used to evaluate the effect of **pyrPOM@PCBM** (inset molecular structure) on the performance of the donor (P3HT)/acceptor (**PCBM**) thin layer OPV device. A bilayer fullerene organization is proposed according to the XRD pattern and the AFM imaging results.

Moreover, the pyrene-tagged building blocks can enable efficient energy transfer to the fullerene cores and shape nano-domains fostering charge transport with enhanced current density and charge collection by the cell electrodes.[30]

The resulting **pyrPOM@PCBM** films show an interesting piezoresponse, typical of ferroelectric materials. Such a behavior was reflected also into a change of **pyrPOM@PCBM** films' optical absorbance of a polarized light and, when incorporated in a bilayer donor/acceptor thin film photovoltaic device (Fig. 1), promotes a significant enhancement of both open circuit voltage and fill factor. Such improvements are further increased when the interlayer is polarized by means of an external bias, recording an increasing of V_{oc} up to 34% in comparison with the classic donor/acceptor configuration.

Results and discussion

Supramolecular adduct characterization

The supramolecular assembly between POM and **PCBM**, (Fig. 1) has been investigated and their mixtures have been characterized.[1,31] The π electrons of the pyrene units are expected to interact with the dense π-electron cloud of the fullerene moiety of **PCBM**.[32]

A solution of **PCBM** in *ortho*-dichlorobenzene (*o*-DCB, 5×10^{-3} M) was added stepwise (4 μL at each step), to a **pyrPOM** dimethylformamide (DMF, 10 μM) solution. The fluorescence spectrum of **pyrPOM**, (350 nm excitation wavelength), shows three bands centered at 379, 397, 405 nm and a shoulder at about 416 nm (Fig. S2b, ESI†).[33] The excimer emission, observed at 450–500 nm, indicates a pyrene-driven aggregation in DMF environment.[34]

Changes in the UV-Vis spectrum are observed in the presence of **PCBM** (Fig. S2a, ESI†) and, simultaneously, a fluorescence quenching of **pyrPOM** (λ_{ex} = 350 nm) is recorded (Fig. S2b, ESI†) as a consequence of the host–guest π–π interaction between the two species.

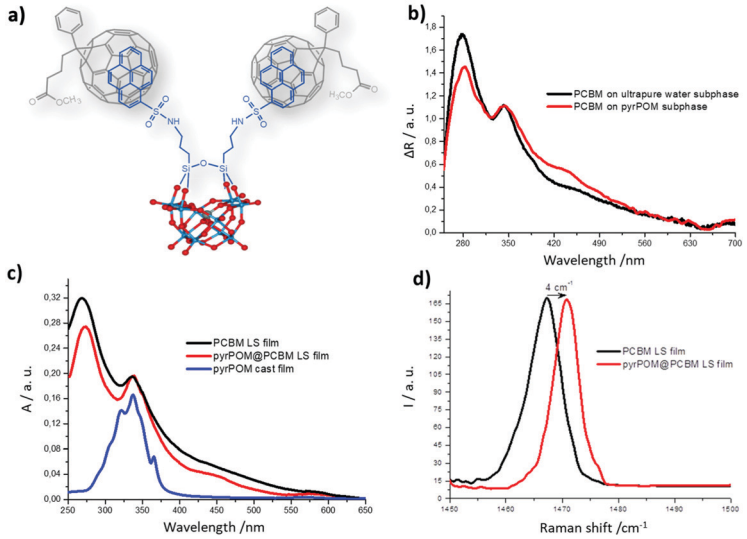

Fig. 2 Chemical structure of **PCBM** and of the polyoxometalate derivative **pyrPOM** forming the supramolecular adduct. In box a, proposed schematization of the supramolecular interaction driven by π–π stacking according to Job's plot derived 1 : 2 stoichiometry. Reflection spectra of **PCBM** and **pyrPOM@PCBM** Langmuir films showing the formation of the supramolecular adduct directly in the floating film (box b). The interaction between the two species is strong enough to ensure the transfer of the **pyrPOM@PCBM** assembly on the solid film (box c) as confirmed by the blue shift of pentagonal pinch mode of the fullerene derivative (box d).

A stoichiometric ratio between **pyrPOM** and **PCBM** of 1 : 2 was calculated by means of the Job's plot (Fig. S2c, ESI†), suggesting the supramolecular arrangement reported in Fig. 2a. A linear Stern–Volmer plot was also obtained monitoring the fluorescence intensity ratio at 397 nm as a function of **PCBM** concentration (Fig. S2d, ESI†), where a binding constant of about 4.38×10^4 M^{-1} was obtained, which is consistent with the expected pyrene-driven host–guest interaction.[28]

The **pyrPOM@PCBM** system and the isolated components were analyzed by cyclic voltammetry (CV) in DMF solution between 1.5 V and −1.7 V (*vs.* Ag/Ag^+, Fig. S3, ESI†). The CV of **PCBM** (1 mM) displays three well defined and reversible mono-electronic reduction waves, showing the typical electron accepting features of the fullerene core, with half-wave potentials, $E_{1/2}$ = −0.246; −0.709; −1.330 V *vs.* Ag/Ag^+.[35] For **pyrPOM** (0.5 mM), the main reduction wave of the hybrid POM scaffold ($E_{1/2}$ = −0.747 V *vs.* Ag^+/Ag^+), is ascribed to the W^{6+}/W^{5+} couple[36] while the irreversible anodic peak with potential, E_{pa} = +1.27 V (*vs.* Ag^+/Ag^+) is due to the oxidation of the pyrene tweezer. The electrochemical behavior of the **pyrPOM@PCBM** is the result of a strong interplay of the two redox active building blocks. As a matter of fact, the characteristic pattern given by the three reversible reduction bands of **PCBM** becomes much less defined, being the first reduction band of PCMB shifted, by the presence of **pyrPOM** donor, towards more negative potentials (−90 mV, see Fig. S3, ESI†).

The formation of a **pyrPOM@PCBM** supramolecular adduct has been promoted directly at the air/water interface of a Langmuir Trough. **PCBM** was dissolved in a chloroform solution with a concentration of 10^{-4} M; a solution of **pyrPOM** (10^{-6} M) in ultrapure water was used as subphase in the Langmuir experiments. The Langmuir–Blodgett (LB) technique and its horizontal variation, the Langmuir–Schaefer (LS) method, were used. These two methods ensure a high control of the deposition parameters, which can be a fundamental aspect for the performance of electronic devices.[37]

The **PCBM** chloroform solution was spread by means of a gas-tight syringe on the surface of the aqueous subphase containing **pyrPOM**. The π–π interaction between the two species is evident by the isotherm curves of the **PCBM** floating film (Fig. S4, ESI†). Furthermore, a comparison between the absorption spectra of the **PCBM** Langmuir film evidences a variation of the ratio between the absorption bands at 344 nm and 277 nm (Fig. 2b). The highlighted band ratio variation confirms the formation of the supramolecular adduct **pyrPOM@PCBM** in the Langmuir film, since only the chromophores migrated at the interface can be detected by the spectrophotometer. The floating film has been transferred by means of the Langmuir–Schaefer method on a quartz substrate. The comparison of UV-Vis spectra registered for **PCBM** deposited from ultrapure water and from the **pyrPOM** containing subphase shows a variation of the band ratio observed for the floating films. This confirms the transfer of the **pyrPOM@PCBM** adduct (Fig. 2c). As a further proof of the supramolecular interaction, the Raman spectra of the LS films of **PCBM** and of the **pyrPOM@PCBM** adduct are compared in Fig. 2d. A 4 cm^{-1} shift towards higher frequencies is observed when the supramolecular adduct is formed. According to the literature, this shift suggests the formation of a supramolecular complex that does not impact on the nature of the fullerene derivatives.[38]

Large areas of the sample surface were scanned by AFM and the morphologies of 1 run LS films of **PCBM** and **pyrPOM@PCBM** appear very different (Fig. 3). **PCBM** thin films partially cover the substrate surface and appear to be formed by small aggregates (Fig. 3A). **pyrPOM@PCBM** film is formed by

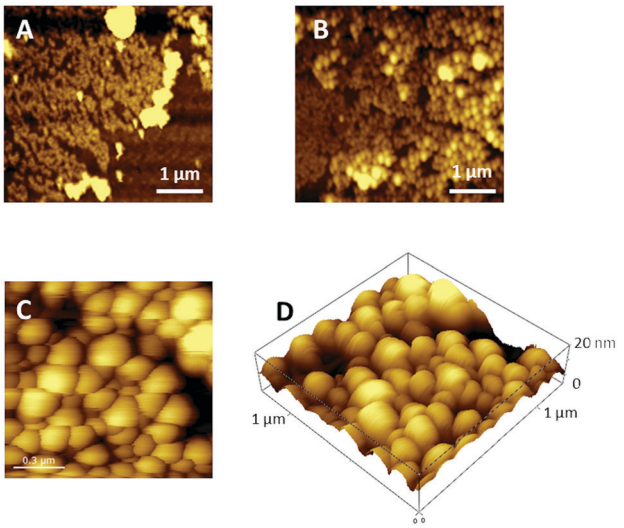

Fig. 3 Topography of **PCBM** (A) and **pyrPOM@PCBM** LS film (deposited by one run, B). (C) A magnification of the globular domains evidences that the size of the aggregates is comprised between 100 and 300 nm. (D) Three-dimensional topography suggests that the aggregates are about 20 nm high.

globular structures arranged in domains of approximately 200 nm (Fig. 3B and C). Furthermore, as reported in Fig. 3D, the aggregates are approximately 20 nm high.

A drastic change of optical parameters of the **pyrPOM@PCBM** film LS film has been recorded by ellipsometry measurements: the optical parameters of the **PCBM** LS film can be fit using two Lorentz oscillators. Instead, the **pyrPOM@PCBM** LS film was studied by two Lorentz oscillators and a Drude model in order to obtain a better data fit (Fig. S5 and S6, ESI†). Furthermore, the Maxwell–Garnett model[39] has been used to evaluate the ratio between **pyrPOM** and **PCBM** within the LS film, where a 1 : 2 ratio was calculated, in agreement with the value obtained in solution (see ESI†). Again, ellipsometry data have been used to estimate the thickness of each transferred LS layer, and a 8.0 ± 0.6 nm thickness was calculated for the LS **pyrPOM@PCBM** film. Such a result has been confirmed by means of X-ray diffraction, carried out in grazing angle configuration (see Fig. 4a). A well-defined peak at 1.2 ± 0.1 degrees indicates a periodicity of 7.6 ± 0.2 nm. On the contrary, the **PCBM** LS film does not show any ordered structure.

Polarizability modulation and opto-electronics behavior

It is particularly interesting to compare the dielectric loss ($\tan\delta$), defined as the ratio between the imaginary and real part of the dielectric function, of the LS films of **pyrPOM@PCBM** and of **PCBM** as a function of the incident electric field (Fig. 4b). The dielectric loss of **PCBM** LS film is very low and monotonically increasing in the range of energy investigated. On the contrary, the dielectric loss of **pyrPOM@PCBM** LS film reaches a maximum value at 375 nm. It may be supposed that, even though the absorption bands of **pyrPOM** and **PCBM** overlap at 375 nm, mainly **pyrPOM** electron clouds are influenced in the charge displacement when the electromagnetic wave is incident on the sample. A possible rationale of such a

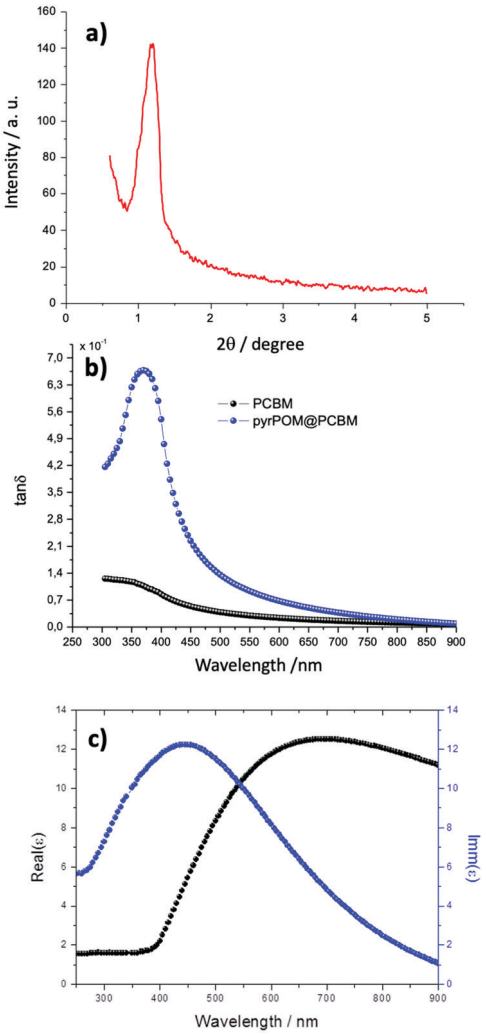

Fig. 4 (a) XRD measurement shows a periodicity of (7.6 ± 0.2) nm of the LS **pyrPOM@PCBM** layer. (b and c) The dielectric loss of **pyrPOM@PCBM**, dramatically different from that one of PCBM, suggests that an electric dipole is created at the opposite edges of the nanodomains. Increasing the frequency, the dielectric permittivity of **pyrPOM@PCBM** LS film becomes negligible.

phenomenon is given considering **pyrPOM@PCBM** as a heterogeneous molecular domain with a semiconducting behavior. An oscillating electric field induces an accumulation of polaron species of opposite charges at the opposite edges of the nanodomain, thus creating an electric dipole. At higher frequencies, polarons cannot follow the electrical field, and the dielectric permittivity becomes negligible (Fig. 4c).[40,41]

As a further characterization, piezoelectric properties of the **pyrPOM@PCBM** LS film have been studied by means of piezoelectric force microscopy (PFM, Fig. S7, ESI†). Two LS runs of **pyrPOM@PCBM** scanned by PFM clearly highlighted the presence of nanograins within the thin film (Fig. S7a, ESI†). Further, the phase difference induced by the piezopotential is very close to 180° (Fig. S7b, ESI†).[42] Such a feature, already observed in LB and LS film of the known ferroelectric polymer P(VDF-TrFE)[43,44] suggests the ferroic nature of the film.

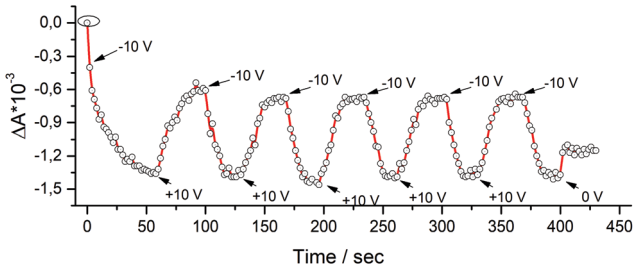

Fig. 5 The absorbance value of **pyrPOM@PCBM** LS film of a *p*-polarized light is dependent on the applied voltage and the optical response is repeatable.

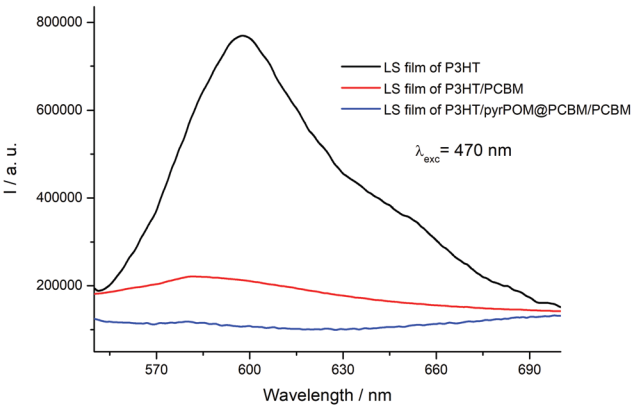

Fig. 6 Fluorescence quenching of the thin film of P3HT emission when transferred on ITO substrate (black line), on ITO/**PCBM** LS film (red line) and on ITO/**PCBM**/**pyrPOM@PCBM**/P3HT stacking (blue line). Excitation wavelength: 470 nm.

Besides, piezoelectric feature proposes such a material as an interesting IFL in organic photovoltaic devices.[29,45,46]

The possibility to modulate the dielectric function and the polarization domain of the **pyrPOM@PCBM** layers, according to the PFM and ellipsometric measurements, was investigated. Absorbance spectra of LS **pyrPOM@PCBM** film, using a *p*-polarized light as incident light (see Fig. 5), were acquired upon alternate application of −10 V and +10 V external bias. The absorbance of the thin film appears directly connected to the applied voltage and the response was reproducible in a series of repeated experiments.

In Fig. 5 the ΔOD of the **pyrPOM@PCBM** LS film under a vertically polarized light at 280 nm has been acquired each 2 seconds, under the application of a voltage, as external trigger. A polarization is induced in the presence of a negative potential (−10 V) that reduces the absorption of the incident polarized light; when the applied voltage is changed in sign (+10 V) the thin film absorbance at 280 nm increases, suggesting that the polarization of the formed dyad is influenced by the external bias, behavior typical of ferroelectric materials.

Donor/acceptor and donor/pyrPOM@PCBM/acceptor photovoltaic devices

Ferroelectric organic and hybrid materials have been largely used for improving the performance of solar devices both as interface layer transferred on the cell electrodes and as interlayer between the donor and the acceptor films. The presence of a ferroelectric interlayer promotes an output photovoltage proportional to the magnitude of the electric polarization.[47–50] It is reported that a direct consequence of the polarized ferroelectric interlayer can significantly enhance the open circuit voltage (V_{oc}) of the solar device.[51,52] A P3HT Langmuir film was formed by spreading 150 μL (10^{-4} M, deposition surface pressure: 14 mN m^{-1}) on ultrapure water subphase and transferred by 15 runs on an ITO substrate by means of the Langmuir–Schaefer method. Then, a **PCBM** Langmuir–Schaefer film (15 runs, spreading volume: 130 μL, deposition surface pressure: 16 mN m^{-1}) was deposited directly onto the ITO/P_3HT structure and the electron charge transfer from the donor layer (P3HT) to the acceptor one (**PCBM**) was monitored by means of fluorescence spectroscopy using an excitation wavelength of 470 nm, corresponding to the maximum absorption of P3HT. The electron transfer from the electron donor to the electron acceptor induces the quenching of the polythiophene derivative fluorescence (Fig. 6).[53] Two LS runs of **pyrPOM@PCBM** were transferred between the P3HT and **PCBM** LS films and the effect of the interlayer on the electronic communication among the donor and acceptor layer was monitored. As reported in Fig. 6, the fluorescence quenching is preserved in the presence of the **pyrPOM@PCBM** interlayer confirming the charge transfer from the polythiophene derivative towards **PCBM** LS layer.

A platinum electrode was evaporated onto the top of the ITO/P3HT/**pyrPOM@PCBM**/**PCBM** structure and an external bias was applied.

The performances of the photovoltaic devices with and without the **pyrPOM@PCBM** interlayer were evaluated (Fig. 7). In agreement with the spectroscopic results, the interlayer does not affect the photocurrent generation improving the open circuit voltage of about 9% if compared with V_{oc} of ITO/P_3HT/**PCBM**/Pt device. In a piezoelectric material the Weiss domains can be aligned using the process of poling, that is the application of an external bias across the material.[54] An external bias of ±5 V was applied across the solar device both in forward (negative pole on Pt electrode) and in reverse (positive pole on Pt electrode) mode.

Poling the ITO/P3HT/**pyrPOM@PCBM**/**PCBM**/Pt device unequivocally improves the efficiency of the solar cell. At the same time the V_{oc} increases from 0.32 V of the ITO/P3HT/**pyrPOM@PCBM**/**PCBM**/Pt without poling up to 0.44 V after poling, increasing the open circuit voltage of about 27%.

Experimental

The **pyrPOM** $(^nBu_4N)_4[\{(C_{16}H_9)SO_2NH(CH_2)_3Si\}_2O(\gamma\text{-}SiW_{10}O_{36})]$ was prepared as previously described.[28]

Cyclic voltammetry experiments were performed by using an Autolab potentiostat/galvanostat (Model 302N) equipped with a three-electrode cell (working electrode: glassy carbon, reference electrode: Ag/AgCl (NaCl 3 M); counter electrode: platinum

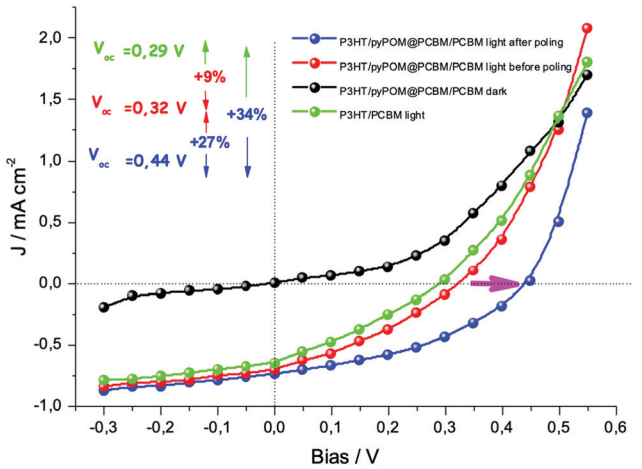

Fig. 7 *J–V* characteristics recorded for solar devices carried out using as photoactive layers P3HT/**PCBM**, P3HT/**pyrPOM@PCBM**//PCBM, P3HT/**pyrPOM@PCBM**//**PCBM** after poling (5 V) under 1.5 AM illumination, black curve is referred to the *J–V* curve of P3HT/**pyrPOM@PCBM**//**PCBM** without the illumination.

wire. In all cases, the samples were dissolved in anhydrous DMF, TBAP (tetrabutylammonium perchlorate) was added as supporting electrolyte (0.10 M), and the solutions were degassed for 15 min under N_2 flow before the measurements. Potentials are expressed with reference to Ag/Ag^+ electrode.

Langmuir experiments and reflection spectra have been carried out by a NIMA500 trough. Barriers' speed was fixed at 5 mm min^{-1} in all the air/subphase interface experiments. All the substrates were cleaned with chloroform/acetone/ethanol/ultrapure water (three times) before use for transferring the Langmuir–Schaefer films.

Ellipsometric measurements have been performed at multiple wavelengths at 55° angle of incidence by means of an EP4 Accurion Instrument. Models used to simulate the optical data are two Lorentz oscillators in the case of **PCBM** film and two Lorentz oscillators and a Drude model for **pyrPOM@PCBM** LS film.

Finally, XRD measurements have been realized by a Rigaku Ultima+ diffractometer in the grazing angle geometry.

Lapped Si/SiO_2 substrate was used to deposit the LS films for the morphological analysis by means of an Atomic and Piezoelectric Force Microscopy (AFM/PFM) instrument (SmartSPM 1000 AIST-NT HORIBA).

UV-Visible spectra on LS films have been recorded by a Cary 5000 equipped with a linear polarizer. Infrared measurements have been carried out by a PerkinElmer Spectrum One with a multireflection tool. Each spectrum was averaged on 64 scans. Fluorescence spectra were recorded using Horiba Fluorolog spectrofluorometer. For IV characterization a Keithley 200 has been used. Raman spectra were recorded by a Horiba Explora microRaman, with an excitation laser of 785 nm.

By means of a Keithley 6517A electrometer the acquisition of the signals output voltage, that derives from the mechanical deformation induced by the movement down-up of an electromagnet driven by a function generator in the 0.01–100 Hz frequency range, has been obtained. To quantitatively evaluate the sensitivity, a microbalance KERN well-defined levels of pressure to the samples has been employed.

For photoelectrical characterization, ITO/(active layer)/I^-, I_3^-/Pt–ITO photoelectrochemical cells were constructed, modifying a previously reported procedure.[55] To prepare the counter electrode, a platinum catalyst was deposited on the ITO glass by coating with 1 drop of a 0.35 mM H_2PtCl_6 solution (2 mg of platinum in 1 mL of ethanol) and heating at 400 °C for 15 min. The electrolyte employed was a solution of 0.5 M LiI and 0.01 M I_2 in acetonitrile. A Keithley 2400 multimeter was used for recording the IV curve and AM 1.5 solar simulator (Quantum Design) was used.

Conclusions

A supramolecular dyad formed by a di-vacant Keggin-type decatungstosilicate bisfunctionalized with pyrene and **PCBM** was assembled by means of π–π interactions between the the fullerene derivative and the pyrene POM and transferred on solid substrates by means of the Langmuir–Schaefer approach. The supramolecular dyad formation was confirmed by means of reflection spectroscopy (at the air/subphase interface), UV-Visible, XRD, fluorescence, ellipsometry and Raman spectroscopy. Furthermore, AFM investigations showed an evident change in the morphology when the LS film of **PCBM** was transferred from the water subphase containing **pyrPOM**. The supramolecular dyad immobilized on solid substrates showed polarization-dependent features that suggest its use for applications in photovoltaic devices. PFM analysis suggests the presence of piezo-responsive nanograins typical of ferroelectric materials. In fact, the dyad film showed absorbance features upon *p*-polarized light excitation sensitive to the application of an external bias. In particular, it was demonstrated that the presence of the **pyrPOM@PCBM** interlayer deposited between a P3HT donor LS film and **PCBM** (as acceptor layer) enhances the V_{oc} of the solar device by about 34% if suitably polarized.

Author contributions

The manuscript was written through contributions of all authors. Gabriele Giancane: data analysis, writing – review and editing. Simona Bettini: data measurement and analysis, writing – original draft; Ludovico Valli: analysis and discussion of experimental results, supervision, writing – review and editing. Victoria Bracamonte: electrochemical experiments. Mauro Carraro: synthesis, writing – review and editing. Marcella Bonchio: analysis and discussion of experimental results, supervision, writing – review and editing. Maurizio Prato: analysis and discussion of experimental results, supervision, writing – review and editing.

Conflicts of interest

There are no conflicts to declare.

Acknowledgements

This research was supported by the PRIN 2017 (protocol number 2017PBXPN4), by the European Innovation Council through the INITIO-FET Project INITIO (Grant Agreement: 828779) and by "Research for Innovation" POR PUGLIA FESR-FSE 2014/2020 Ricerca Regione Puglia. Part of this work was performed under the Maria de Maeztu Units of Excellence Program from the Spanish State Research Agency Grant No. MDM-2017-0720.

References

1 J. C. Hummelen, B. W. Knight, F. Lepeq, F. Wudl, J. Yao and C. L. Wilkins, *J. Org. Chem.*, 1995, **60**, 532–538.
2 H. Lee, C. Park, D. H. Sin, J. H. Park and K. Cho, *Adv. Mater.*, 2018, **30**, 1800453.
3 L. Dou, J. You, Z. Hong, Z. Xu, G. Li, R. A. Street and Y. Yang, *Adv. Mater.*, 2013, **25**, 6642–6671.
4 D. H. Wang, A. K. K. Kyaw, J. R. Pouliot, M. Leclerc and A. J. Heeger, *Adv. Energy Mater.*, 2014, **4**, 1300835.
5 K. M. Pelzer and S. B. Darling, *Mol. Syst. Des. Eng.*, 2016, **1**, 10–24.
6 S. Few, J. M. Frost and J. Nelson, *Phys. Chem. Chem. Phys.*, 2015, **17**, 2311–2325.
7 T. M. Clarke and J. R. Durrant, *Chem. Rev.*, 2010, **110**, 6736–6767.
8 J. Yu, Y. Zheng and J. Huang, *Polymers*, 2014, **6**, 2473–2509.
9 S. H. Liao, Y. L. Li, T. H. Jen, Y. S. Cheng and S. A. Chen, *J. Am. Chem. Soc.*, 2012, **134**, 14271–14274.
10 J. H. Seo, A. Gutacker, Y. Sun, H. Wu, F. Huang, Y. Cao, U. Scherf, A. J. Heeger and G. C. Bazan, *J. Am. Chem. Soc.*, 2011, **133**, 8416–8419.
11 M. Carraro, G. Bergamini, M. Di Lauro, G. Modugno, M. Baroncini, P. Ceroni and M. Bonchio, *Eur. J. Inorg. Chem.*, 2016, 3405–3410.
12 Z. Syrgiannis, G. Trautwein, M. Calvaresi, G. Modugno, F. Zerbetto, M. Carraro, M. Prato and M. Bonchio, *Eur. J. Inorg. Chem.*, 2019, 374–379.
13 L. C. Palilis, M. Vasilopoulou, D. G. Georgiadou and P. Argitis, *Org. Electron.*, 2010, **11**, 887–894.
14 M. Vasilopoulou, A. M. Douvas, L. C. Palilis, S. Kennou and P. Argitis, *J. Am. Chem. Soc.*, 2015, **137**, 6844–6856.
15 L. C. Palilis, M. Vasilopoulou, A. M. Douvas, D. G. Georgiadou, S. Kennou, N. A. Stathopoulos, V. Constantoudis and P. Argitis, *Sol. Energy Mater. Sol. Cells*, 2013, **114**, 205–213.
16 M. Vasilopoulou, E. Polydorou, A. M. Douvas, L. C. Palilis, S. Kennou and P. Argitis, *Energy Environ. Sci.*, 2015, **8**, 2448–2463.
17 X. Jia, L. Shen, M. Yao, Y. Liu, W. Yu, W. Guo and S. Ruan, *ACS Appl. Mater. Interfaces*, 2015, **7**, 5367–5372.
18 Y. Zhu, Z. Yuan, W. Cui, Z. Wu, Q. Sun, S. Wang, Z. Kang and B. Sun, *J. Mater. Chem. A*, 2014, **2**, 1436–1442.
19 M. Alaaeddine, Q. Zhu, D. Fichou, G. Izzet, J. E. Rault, N. Barrett, A. Proust and L. Tortech, *Inorg. Chem. Front.*, 2014, **1**, 682–688.
20 M. Tountas, Y. Topal, E. Polydorou, A. Soultati, A. Verykios, A. Kaltzoglou, T. A. Papadopoulos, F. Auras, K. Seintis, M. Fakis, L. C. Palilis, D. Tsikritzis, S. Kennou, M. Koutsoureli, G. Papaioannou, M. Ersöz, M. Kus, P. Falaras, D. Davazoglou, P. Argitis and M. Vasilopoulou, *ACS Appl. Mater. Interfaces*, 2017, **9**, 22773–22787.
21 B. A. Collins, Z. Li, J. R. Tumbleston, E. Gann, C. R. Mcneill and H. Ade, *Adv. Energy Mater.*, 2013, **3**, 65–74.
22 J. Guo, H. Ohkita, H. Benten and S. Ito, *J. Am. Chem. Soc.*, 2010, **132**, 6154–6164.
23 P. Westacott, J. R. Tumbleston, S. Shoaee, S. Fearn, J. H. Bannock, J. B. Gilchrist, S. Heutz, J. Demello, M. Heeney, H. Ade, J. Durrant, D. S. McPhail and N. Stingelin, *Energy Environ. Sci.*, 2013, **6**, 2756–2764.
24 S. Sweetnam, K. R. Graham, G. O. Ngongang Ndjawa, T. Heumüller, J. A. Bartelt, T. M. Burke, W. Li, W. You, A. Amassian and M. D. McGehee, *J. Am. Chem. Soc.*, 2014, **136**, 14078–14088.
25 S. Mukherjee, X. Jiao and H. Ade, *Adv. Energy Mater.*, 2016, **6**, 1600699.
26 W. Chen, T. Xu, F. He, W. Wang, C. Wang, J. Strzalka, Y. Liu, J. Wen, D. J. Miller, J. Chen, K. Hong, L. Yu and S. B. Darling, *Nano Lett.*, 2011, **11**, 3707–3713.
27 D. Baran, R. S. Ashraf, D. A. Hanifi, M. Abdelsamie, N. Gasparini, J. A. Röhr, S. Holliday, A. Wadsworth, S. Lockett, M. Neophytou, C. J. M. Emmott, J. Nelson, C. J. Brabec, A. Amassian, A. Salleo, T. Kirchartz, J. R. Durrant and I. McCulloch, *Nat. Mater.*, 2017, **16**, 363–369.
28 G. Modugno, Z. Syrgiannis, A. Bonasera, M. Carraro, G. Giancane, L. Valli, M. Bonchio and M. Prato, *Chem. Commun.*, 2014, **50**, 4881–4883.
29 B. Yang, Y. Yuan, P. Sharma, S. Poddar, R. Korlacki, S. Ducharme, A. Gruverman, R. Saraf and J. Huang, *Adv. Mater.*, 2012, **24**, 1455–1460.
30 B. Kadem, E. N. Kaya, A. Hassan, M. Durmuş and T. Basova, *Sol. Energy*, 2019, **189**, 1–7.
31 M. C. Scharber, D. Mühlbacher, M. Koppe, P. Denk, C. Waldauf, A. J. Heeger and C. J. Brabec, *Adv. Mater.*, 2006, **18**, 789–794.
32 F. M. Toma, A. Sartorel, M. Iurlo, M. Carraro, S. Rapino, L. Hoober-Burkhardt, T. Da Ros, M. Marcaccio, G. Scorrano, F. Paolucci, M. Bonchio and M. Prato, *ChemSusChem*, 2011, **4**, 1447–1451.
33 J. González-Benito, J. C. Cabanelas, A. Aznar, M. R. Vigil, J. Bravo, B. Serrano and J. Baselga, *J. Lumin.*, 1997, **72–74**, 451–453.
34 F. Winnik, *Chem. Rev.*, 1993, **93**, 587–614.
35 G. D. Han, W. R. Collins, T. L. Andrew, V. Bulović and T. M. Swager, *Adv. Funct. Mater.*, 2013, **23**, 3061–3069.
36 G. Modugno, A. Monney, M. Bonchio, M. Albrecht and M. Carraro, *Eur. J. Inorg. Chem.*, 2014, 2356–2360.
37 T. L. Penner, H. R. Motschmann, N. J. Armstrong, M. C. Ezenyilimba and D. J. Williams, *Nature*, 1994, **367**, 49–51.
38 M. Behera and S. Ram, *J. Inclusion Phenom. Macrocyclic Chem.*, 2012, **72**, 233–239.

39 M. Y. Koledintseva, S. K. R. Chandra, R. E. DuBroff and R. W. Schwartz, *Prog. Electromagn. Res.*, 2006, **66**, 213–228.
40 S. Dang, *J. Phys. D: Appl. Phys.*, 2008, **41**, 125101.
41 W. Hu, L. Li, W. Tong, G. Li and T. Yan, *J. Mater. Chem.*, 2010, **20**, 8659–8667.
42 C. Liu, J. Ma, J. Ma, Y. Zhang, J. Chen and C. W. Nan, *AIP Adv.*, 2017, **7**, 055003.
43 P. Sharma, T. Reece, D. Wu, V. M. Fridkin, S. Ducharme and A. Gruverman, *J. Phys.: Condens. Matter*, 2009, **21**, 485902.
44 P. Sharma, A. Fursina, S. Poddar, S. Ducharme and A. Gruverman, *Appl. Phys. Lett.*, 2014, **105**, 182903.
45 C. R. Bowen, H. A. Kim, P. M. Weaver and S. Dunn, *Energy Environ. Sci.*, 2014, **7**, 25–44.
46 M. Zheng, Q. Xu, R. Tian and C. Lu, *J. Colloid Interface Sci.*, 2021, **600**, 473–479.
47 Y. Yuan, Z. Xiao, B. Yang and J. Huang, *J. Mater. Chem. A*, 2014, **2**, 6027–6041.
48 Y. Hu, F. Florio, Z. Chen, W. Adam Phelan, M. A. Siegler, Z. Zhou, Y. Guo, R. Hawks, J. Jiang, J. Feng, L. Zhang, B. Wang, Y. Wang, D. Gall, E. F. Palermo, Z. Lu, X. Sun, T. M. Lu, H. Zhou, Y. Ren, E. Wertz, R. Sundararaman and J. Shi, *Sci. Adv.*, 2020, **6**, eaay4213.
49 R. R. Bai, C. R. Zhang, Z. J. Liu, X. K. Chen, Y. Z. Wu, W. Wang and H. S. Chen, *Comput. Theor. Chem.*, 2020, **1186**, 112914.
50 L. Hu, S. Dalgleish, M. M. Matsushita, H. Yoshikawa and K. Awaga, *Nat. Commun.*, 2014, **5**, 3279.
51 S. Y. Yang, J. Seidel, S. J. Byrnes, P. Shafer, C. H. Yang, M. D. Rossell, P. Yu, Y. H. Chu, J. F. Scott, J. W. Ager, L. W. Martin and R. Ramesh, *Nat. Nanotechnol.*, 2010, **5**, 143–147.
52 T. Ahamad, A. Aldalbahi, S. M. Alshehri, S. Alotaibi, S. Alzahly, Z. B. Wang and P. X. Feng, *Sol. Energy*, 2021, **220**, 758–765.
53 S. Bettini, S. Sawalha, L. Carbone, G. Giancane, M. Prato and L. Valli, *Nanoscale*, 2019, **11**, 7414–7423.
54 A. Roberts and R. Romanofsky, *Integrated Ferroelectrics*, Taylor & Francis Group, 2012, vol. 134, pp. 102–110.
55 S. Ito, T. N. Murakami, P. Comte, P. Liska, C. Grätzel, M. K. Nazeeruddin and M. Grätzel, *Thin Solid Films*, 2008, **516**, 4613–4619.